

Mercury Emission to the Atmosphere from Experimental Manipulation of DOC and UVR in Mesoscale Field Chambers in a Freshwater Lake

STEPHEN C. PETERS,*
JENNIFER L. WOLLENBERG,
DONALD P. MORRIS, AND
JASON A. PORTER

Department of Earth and Environmental Sciences, Lehigh University, Bethlehem, Pennsylvania 18015

Mesocosm experiments in an optically transparent lake allow the manipulation of both dissolved organic carbon (DOC) and incident ultraviolet radiation (UVR) in order to study mercury reduction and emission processes. In the absence of UVR and the presence of visible light, mercury emission is very low (~ 0.3 ng/m²/h). When UVR is permitted in the mesocosm chambers, mercury emission increases, with emission rates ranging from 0.3 to 2.5 ng/m²/h. At concentrations between 1.5 and 2.5 mg/L DOC, mercury emission does not appear to depend on either the concentration or the optical properties of the DOC. In particular, the addition of 1.0 mg/L DOC from a nearby wetland to a photobleached mesocosm did not increase the emission of mercury. The similarities between mercury emission from highly photobleached 1.5 mg/L DOC and from terrestrially enriched 2.5 mg/L DOC suggest that the moieties responsible for mercury reduction are far in excess of that needed for mercury reduction. Using the measured flux rate of mercury from the water surface, we calculated a dissolved gaseous mercury (DGM) concentration that would need to be present to drive the emissive flux. The buildup of DGM was used to approximate a kinetic rate constant for the net mercury reduction in this system of approximately 0.17 h⁻¹, which is consistent with existing published values.

Introduction

The transport of inorganic Hg between the Earth's surface and the atmosphere is dominated by the reduction of aqueous Hg species to Hg⁰, which volatilizes across the air/water interface. Once in the atmosphere, Hg⁰ can be oxidized to Hg^{II}, which then reacts with particulates and aerosols and is deposited back to the Earth's surface. Fluxes between the major Earth reservoirs have been the topic of considerable study (1–6).

The emission rate of Hg from water bodies is governed by the production of dissolved gaseous mercury (DGM) in the water column and the transport of this sparingly soluble vapor to the water surface. The production of DGM is the net sum of the forward and reverse rates of the following redox

reaction: $\text{Hg}^{\text{II}} + 2\text{e}^- \rightleftharpoons \text{Hg}^0$. The overall reduction is generally observed in most natural systems and is likely coupled primarily to dissolved organic carbon (DOC) oxidation (e.g., 7, 8). The direct photooxidation of Hg⁰ to Hg^{II} by ultraviolet radiation (UVR) may be an important mechanism that can decrease the net production of DGM and therefore the flux of Hg from the water column to the atmosphere (9). In freshwater and riverine systems, production of DGM seems to be driven by DOC photoreactions (e.g., 10, 11) and by microbial activity regulated by the photochemical production of hydrogen peroxide (12). Once DGM is produced, it can either be emitted to the atmosphere or directly or indirectly reoxidized in the water column (9).

The chemical transformations relevant to the air/water exchange of mercury are dependent on hypothesized coupled reactions that occur during the photolysis of chromophoric DOC. These compounds strongly absorb UVR and are subject to photolysis, which can change their chemical nature and thus alter potential binding sites for Hg^{II}. Photolysis of organic matter also causes changes in its optical properties (absorbance and fluorescence), which can be monitored in the field or the laboratory. Changes in DOC fluorescence have been suggested as a proxy for DGM formation rates in boreal lakes (13). Increasing emission of Hg⁰ as a function of DOC concentration has also been observed in laboratory experiments for seawater (7, 14) and freshwater samples (15, 16).

The most significant impact of UVR on Hg reduction is through coupled oxidation of DOC, as described above. The reduction of Hg^{II} has been well studied, including the investigation of the effects of DOC concentration, light intensity, and wavelength (7, 17, 18). Increased rates of transformation of Hg^{II} to Hg⁰ were observed at higher concentrations of DOC, at higher light intensity, and at smaller wavelengths of UVR. Direct photooxidation of mercury has also been observed to occur, most likely the result of reaction with a photoproduct reactive intermediate (9). The commonly observed diel cycles of mercury emission are generally positively correlated to intensity of solar radiation (19, 20), although some studies demonstrate only a weak relationship with light intensity (21) that can be explained by a lag time between DGM production and volatilization (22).

In this paper, we report on a field experiment designed to test the influence of controlling natural incident UVR and manipulating the concentration of DOC within an in situ experimental water column complete with an aquatic foodweb. We plan to explain the observed differences in mercury flux are primarily due to the presence or absence of UVR and to a much smaller degree by DOC concentration.

Experimental Section

Twelve cylindrical mesocosms were fabricated from transparent flexible plastic materials that either blocked UVR (Courtgard, Solutia, Inc., Martinsville, VA) or permitted UVR to pass (Aclar, Honeywell, Pottsville, PA). The UVR blocking material absorbs 97% of the radiation from 290–400 nm while the UVR transmissive material allows 87+% of the energy above ~ 250 nm (Figure SI-1, Supporting Information). Mesocosms were approximately 0.74 m in diameter and 8 m deep to encompass the photic zone, for a total volume of 3440 L. These mesocosms were suspended on floating racks in Lake Giles (41°22' N, 75°05' W, Figure SI-2, Supporting Information) so that the mesocosm chamber walls extended approximately 30 cm above the lake surface to block surface wind and keep lake water from entering the chambers. The tops of the chambers were covered at a height of ~ 50 cm

* Corresponding author phone: (610) 758-3957; fax: (610) 758-3677; e-mail: scp2@lehigh.edu.

above the water surface with the same materials used to construct the chambers. The gap of ~20 cm on all sides allows free gas exchange between the atmosphere and the mesocosm environment. Mesocosms were filled with lake water passed through a 102 µm mesh screen to remove zooplankton. Tows of zooplankton from the lake were then added to each mesocosm individually to ensure a consistent foodweb structure. Dissolved organic matter was concentrated from Beaver Pond using a reverse osmosis system (Desal, GE Osmonics), which has an exclusion efficiency of 95% between a molecular weight of 70 and 100, and does not concentrate inorganic ions. The DOC concentrate was refiltered to 0.22 µm (Memtrex Filter, GE Osmonics, Inc.) and then added to six of the mesocosms to attain a final concentration of ~2.5 mg/L, which is at the low end of natural water DOC concentrations, so as to enable observations of slightly DOC-limited photoreactions. The DOC concentrated from Beaver Pond is similar to that transported into Lake Giles from terrestrial allochthonous sources. The remaining six mesocosms contained Giles lake water with unamended DOC at an ambient concentration of ~1.5 mg/L. The DOC concentration in the mesocosms did not change appreciably during the course of the experiment, except in the +UV, 2.5 mg/L treatment, where the concentration dropped to 2.3 mg/L by the end of the experimental period. The pH and conductivity of mesocosms with DOC amendments did not differ significantly from those filled only with water from Lake Giles, suggesting that the manipulation did not strongly influence inorganic ion concentrations. No mercury was “spiked” or “amended” to any of the mesocosms. Dissolved Hg^{II} concentrations averaged 1.80 and 1.77 ng/L in the 2.5 mg/L, ±UV treatments, respectively, with no significant upward or downward trend over the experimental period. For the purposes of discussion, the DOC treatments are referred to by their concentrations, and the UVR treatments are referred to by whether they passed (+) or excluded (–) UVR. The combination of +UVR/–UVR and 1.5 and 2.5 mg/L DOC parameters follows a 2 × 2 factorial matrix with three replicates. Mercury flux was measured and reported for only one of the three sets of replicate mesocosms due to the single-channel mercury analyzer available for the project.

Mercury emission rates were measured using a flux chamber and continuous mercury monitor. The flux chamber was modeled after literature procedures (23, 24) and was approximately 42 cm in diameter and 20 cm in height. The chamber was constructed from acrylic and polyethylene materials with measured UV-B transmission rates greater than 85%. Eight holes, each approximately 4 mm in diameter, were drilled at 45° degree intervals around the circumference of the chamber, approximately 3 cm above the water surface. The chambers were continuously pumped at a rate of 0.6 L/min during the day. Elemental gaseous mercury concentration was determined with gold amalgamation and absorbance detection using a field portable instrument (Mercury Instruments UT-3000). Ambient mercury concentration was measured at the inlet to the chamber, and the overall mercury flux rate was calculated using the following equation

$$J_{\text{Hg}} = (C_i - C_0) \left(\frac{Q}{A} \right) \quad (1)$$

Where J_{Hg} is the calculated mercury flux, C_i and C_0 are the chamber and ambient mercury concentrations, respectively, Q is the sampling flow rate, and A is the open aperture of the chamber. Fluxes calculated using this equation are expressed in units of ng/m²/hr for the purposes of discussion within the text.

An estimate of the dissolved gaseous mercury concentrations in the water column was calculated from the following equation (7, 25)

$$E = -K \left(\frac{C_a}{H} - C_w \right) \quad (2)$$

where E is the mercury flux (ng/m²/h), K is the piston velocity (m/h), H is the Henry's Law constant for Hg⁰ (26), and C_a and C_w are the gaseous mercury concentrations in air and water, respectively. In our case, we have the measured flux rate and need to estimate the formation of dissolved gaseous mercury in the water (C_w). Solving eq 2 for this term gives

$$C_w = \frac{C_a}{H} + \frac{E}{K} \quad (3)$$

We used field temperature data to calculate H (26) and mean wind speed to estimate K (7). Atmospheric mercury concentration (C_a) was fixed at 2 ng/m³, which is equivalent to the average of >3 values measured daily at ~10 cm above the lake surface during the experimental period. Data calculated using this approach are subject to absolute errors as a result of inaccuracies in the estimation of the piston velocity under varying wind and wave conditions. However, we use the rate of ingrowth of DGM (eq 4) instead of the absolute values to calculate a net rate constant, which mathematically eliminates these possible errors.

$$k = \frac{\ln([\text{Hg}_t]/[\text{Hg}_0])}{t - t_0} \quad (4)$$

Incident UVR was measured using an SR-18 UV-B radiometer. The radiometer measures cosine-corrected incident radiation from 290 to 324 nm over 16 discrete wavebands with a ~2 nm half-power bandwidth. UV-A and visible wavelengths are estimated with a radiative transfer model and are considered accurate to ~5% (27).

DOC photobleaching was monitored in each of the mesocosms during the study by measuring a variety of optical parameters, some of which are specific indicators of photobleaching. Measurements of dissolved absorbance (a_d) were made on filtered (Whatman GF/F) samples using a Shimadzu UV-Vis 1601 dual-beam spectrophotometer (200–800 nm) and a 1 or 10 cm quartz Supersil cuvette referenced to air. Spectral slope (S) was calculated as the slope of the log transform of absorbance for UV-A (320–400 nm) and UV-B (280–320 nm) wavelengths. DOC specific absorbance was calculated by dividing the absorption coefficient (a , m⁻¹) by the DOC concentration (mg/L). Both the spectral slope and the DOC specific absorbance provide an index of the degree of DOC photobleaching (28). Fluorescence was measured on filtered samples (Whatman GF/F) using a Shimadzu RF-551 fluorometer. Emission intensity was measured for the entire visible spectrum (400–700 nm) using an excitation wavelength of 370 nm. A blank was subtracted from the spectrum and 10 point averages centered on 450 and 500 nm were used to calculate the fluorescence index (29). DOC was measured on a Shimadzu TOC-V instrument (Columbia, MD) using the considerations outlined by Sharp (30).

Results

Initial Mercury Emission. Mercury emission rates from the mesocosms to the atmosphere ranged from 0.19 to 2.5 ng/m²/hr across all treatments for the entire experimental period (Figure 1). We measured mercury flux close to solar noon on each day we had access to the site. Those data are represented in Figure 1 by either a single measurement or a grouping of measurements on a given date. On selected dates in the middle of the experimental period, we were able to measure the flux commencing at dawn and throughout the day. At the beginning of the experiment, mercury flux maxima ranged from 0.31 to 0.83 ng/m²/h in the 1.5 and 2.5 mg/L DOC,

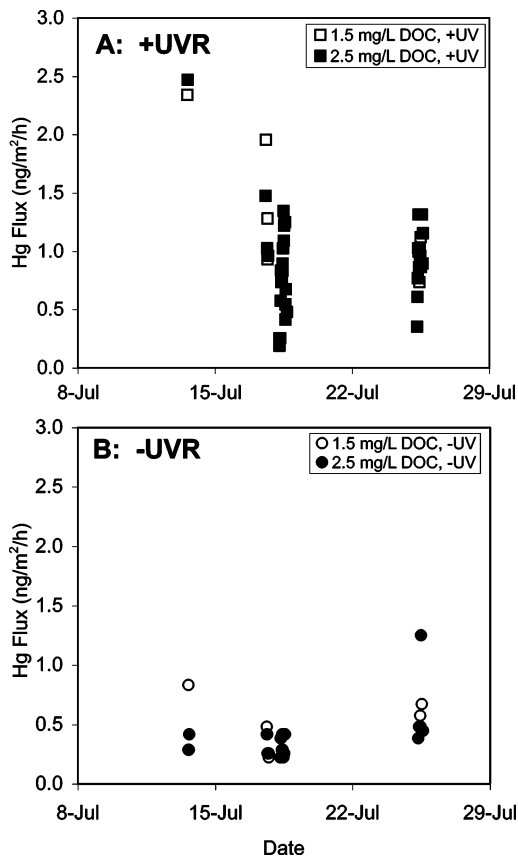


FIGURE 1. Summary of mercury flux data for the +UV treatments (A) and the -UV treatments (B). Open and filled symbols represent 1.5 and 2.5 mg/L DOC treatments, respectively. Multiple measurements on several days are indicated by the vertical clusters of points.

-UVR treatments, respectively (Figure 1B). Mercury flux maxima in the 1.5 and 2.5 mg/L DOC, +UVR treatments were considerably higher ($p < 0.001$, Mann-Whitney), ranging from 2.3 to 2.5 $\text{ng}/\text{m}^2/\text{h}$ respectively (Figure 1A). The initial flux of mercury from the mesocosms did not appear to differ between experimental treatments at DOC concentrations of 1.5 and 2.5 mg/L.

Diel Fluctuations. Time series measurements of mercury flux were measured on two days in the middle of the experimental period and appear as narrow vertical clusters of datapoints in Figure 1. These data were expanded and plotted for these two dates in Figure 2 along with measured incoming UV-B irradiance. On July 19, mercury flux from the +UVR mesocosm ranged from near zero to a maxima of 1.35 $\text{ng}/\text{m}^2/\text{h}$ (Figure 2A). Mercury flux tracks closely with incoming UV-B in the morning, but then the flux rate drops in the afternoon before the UV-B diminishes. Brief periods of diminished UV-B irradiance after 13:00 hours were due to scattered clouds that moved into the area. Mercury emission from the -UVR treatment did not appreciably rise during the course of the diel measurement period. On July 26, mercury emission in the +UVR mesocosm followed a similar pattern to that observed on July 19 (Figure 2B), though the rise in UV-B irradiance for that time period was slightly diminished in magnitude and delayed compared with that of July 19. Flux from the +UVR mesocosm remained high throughout most of the midday hours and was more independent of UV-B irradiance than on the previous measurement date. Mercury flux from the -UVR mesocosm remained at predawn values for the day, similar to the observations from the July 19 diel observations.

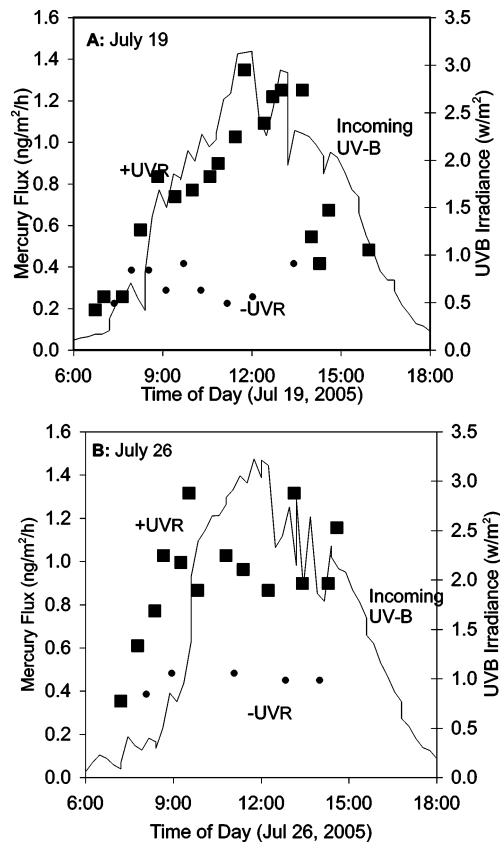


FIGURE 2. Diel fluctuations in mercury flux in the +UVR (squares) and -UVR (circles) on two separate days. UV-B irradiance (line) is plotted for comparison.

A closer examination of the mercury flux rates compared to UV-B irradiance can be obtained by plots of these two variables (Figure 3). For the data collected on July 19, mercury flux rates follow a linear relation with UV-B irradiance ($R^2 = 0.69$, Figure 3A). If the last four points are excluded from the regression, the correlation coefficient improves to 0.87 with no appreciable change in slope ($\sim 0.34 \text{ ng}/\text{hr}/\text{w}$). On the second sampling date, the relationship between flux and UV-B irradiance is less consistent (Figure 3B). In the early morning, mercury flux increased rapidly, reaching the maximum for the day of approximately 1.3 $\text{ng}/\text{m}^2/\text{h}$ by $\sim 09:30$ hours. The slope of this initial rise in mercury flux is approximately 3 times more rapid than that observed on the previous date (1.1 $\text{ng}/\text{hr}/\text{w}$). For the remainder of the day, mercury flux varied irrespective of UV-B irradiance, ranging from 0.86 to 1.3 $\text{ng}/\text{m}^2/\text{h}$.

Experimental Progression. Peak mercury fluxes, measured close to solar noon on each of the experimental days were determined and plotted vs time (Figure 4). In the +UVR treatments, peak mercury flux declined from $\sim 2.4 \text{ ng}/\text{m}^2/\text{h}$ down to $\sim 1.2 \text{ ng}/\text{m}^2/\text{h}$ over the course of the 12 day experimental period (Figure 4). Peak emissions from the two +UVR mesocosms were nearly identical at the beginning, with the 2.5 mg/L DOC mesocosm emitting 2.5 $\text{ng}/\text{m}^2/\text{h}$, compared to the 1.5 mg/L DOC treatment emitting 2.3 $\text{ng}/\text{m}^2/\text{h}$. The 2.5 mg/L DOC treatment decreased in emission rate to $\sim 1.5 \text{ ng}/\text{m}^2/\text{h}$ after the first week of the experiment, while the 1.5 mg/L DOC treatment declined only half as much, to $\sim 2 \text{ ng}/\text{m}^2/\text{h}$. In this same period, DOC absorbance in the +UVR treatment decreased the largest amount, from 5.8 to 5.0 m^{-1} , most likely from photobleaching. Near the end of the experiment, flux rates converged to a value of $\sim 1.2 \text{ ng}/\text{m}^2/\text{h}$. In comparison, the -UVR treatments had considerably lower fluxes that remained constant through

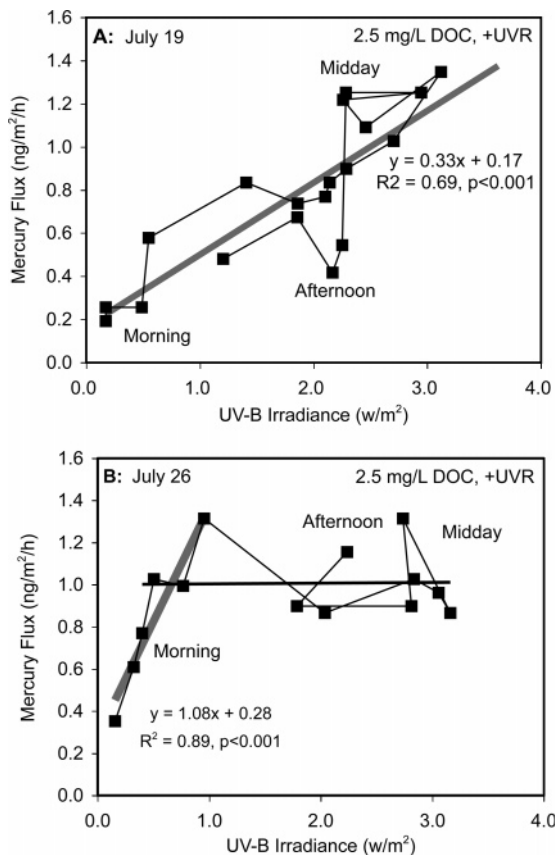


FIGURE 3. Plots of mercury flux vs UV-B irradiance for two different dates. Linear regressions (gray lines) are significant at $p < 0.001$. In the lower graph, a regression through all data except the first two points has zero slope (black line), possibly indicating that flux is independent of irradiance.

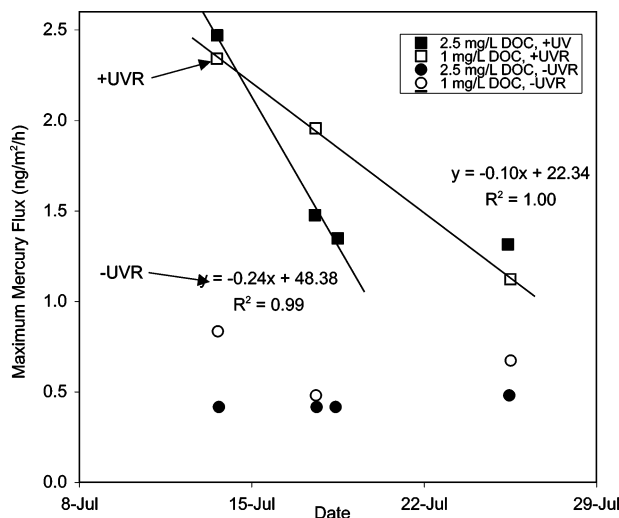


FIGURE 4. Plot of peak mercury flux vs time. Regressions are plotted through all dates of the 1 mg/L DOC treatment (open squares) and the first three points of the 2.5 mg/L DOC treatment (filled squares). Both regressions are significant at $p < 0.001$. Flux rates do not exhibit significant change in the $-UVR$ treatment (circles).

the experimental period (Figure 4). Mean peak flux for all treatments was ~ 0.5 ng/m²/h, with the highest value of 0.83 ng/m²/h observed at the beginning of the experiment in the 1.5 mg/L DOC, $-UVR$ treatment.

Optical Properties. Total fluorescence measured in water (450–600 nm) from the mesocosms ranged from 7000 in the 2.5 mg/L DOC treatment down to 1650 in the 1.5 mg/L DOC

treatment (Figure 5A). Fluorescence declined approximately 25% during the course of the experiment in the 2.5 mg/L DOC treatment but did not change in the 1.5 mg/L DOC treatment. The fluorescence index (450:500 nm) averaged 1.35 ± 0.02 for the 2.5 mg/L DOC treatment during the entire experiment (Figure 5B). Fluorescence index data for the 1.5 mg/L DOC treatment starts at a value of 1.75, drops to a value of 1.57 on July 14, and then returns to a value of 1.72 by the end of the experiment.

Absorbance measurements at 320 nm in the 2.5 mg/L treatment decrease 25% during the course of the experiment, from 6.0 to 4.5 m⁻¹, while the 1.5 mg/L treatment remained constant at ~ 1.0 m⁻¹ (Figure 5C). The DOC specific absorbance measured at 320 nm decreases from a value of 2.5 to a value of 1.9 in the 2.5 mg/L treatment, while the 1.5 mg/L DOC treatment remains constant at ~ 0.7 (Figure 5D). The UV-B spectral slope remained moderately constant throughout the experiment, with the 2.5 and 1.5 mg/L DOC treatments having mean values of -0.015 ± 0.0005 and -0.023 ± 0.0007 , respectively.

Discussion

DOC Effects on Emission. In this project, we manipulated both DOC concentration and the spectral properties of incoming light, without adding mercury to the system. The manipulation of DOC by supplementing the starting concentration of 1.5 mg/L with an additional 1 mg/L of DOC did not appear to have a significant effect on the initial mercury fluxes from the mesocosms (Figure 1A). Two fluxes measured on the first day of the experiment were 2.3 and 2.5 ng/m²/h and differ by only 8.3%. Unfortunately, the flux from the 1.5 mg/L DOC mesocosm was only measured once on that initial day due to experimental constraints, and therefore, statistical analysis is not feasible. However, given a total analytical uncertainty of approximately 5% along with deviations in peak mercury intensity observed on other days of 5–10%, it is very unlikely that the observed fluxes on the first day were significantly different between the 1.5 and 2.5 mg/L treatments. This observation is consistent with results obtained by other researchers, whereby small increases in DOC concentration do not correspond to a linear increase in mercury photoreduction rate (7, 14). Larger increases in DOC (2–14 mg/L) have been observed to produce more DGM, though they require approximately 10 times the amount of DOC to double the DGM production (10). Future experiments at this scale would need to use considerably more and/or different types/isolates of DOC to produce more dramatic differences.

Irradiation Effects on Emission. The diel cycle in incoming solar radiation is a useful tool for studying the radiation-induced variations in gaseous mercury flux. We assume that net UV photoreduction commences at sunrise, then during the morning hours, increasing solar radiation creates a buildup of DGM in the water column. The increase in DGM would result in observable increases in net mercury flux as the day proceeds. After solar noon, the photoreduction decreases, and the DGM pool diminishes proportionally, but perhaps with a lag related to the rate constants of the two competing reactions. Evidence of this process will be net photoreduction rates that are consistent with existing experimental data.

On the two days when the flux was measured continuously throughout the diel cycle, flux measurements followed similar overall trends, with subtle differences observed in the strength of the relation between UV-B and mercury flux levels. On July 19, a mostly linear relationship was observed, with peak radiation corresponding to peak mercury emission ($R^2 = 0.69$, $p < 0.0001$). We did not observe a plateau in the peak mercury flux at any irradiance value. The system in this condition might be UVR limited, and we might expect that incremental

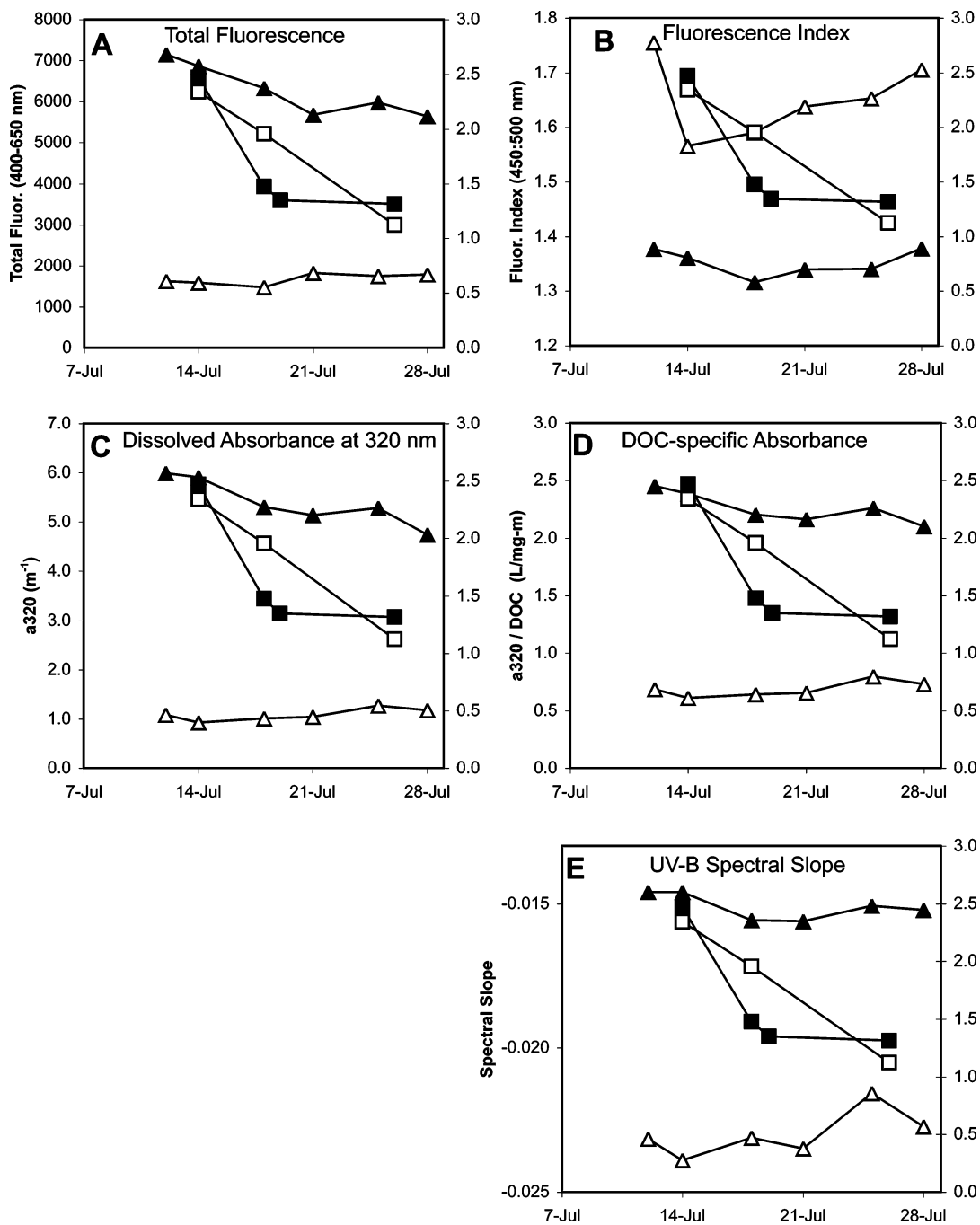


FIGURE 5. Comparison of mercury flux rates to the temporal evolution of the optical properties of +UVR treatment mesocosms. Square symbols correspond to the right-hand axis with mercury flux rates in $\text{ng}/\text{m}^2/\text{h}$. Triangular symbols correspond to the left-hand axis and have the units of the relevant optical property. For both parameters, filled symbols represent the 2.5 mg/L DOC mesocosm, and the open symbols represent the 1.5 mg/L DOC mesocosm.

increases in UVR might produce more emission. On July 26, mercury flux increased more rapidly at daybreak, but then did not track as closely with incoming radiation for the remainder of the day. A regression through the first six datapoints is significant ($R^2 = 0.89$, $p < 0.0001$), though it has a slope more than 3 times steeper than that observed on July 19. The steepness of this section of the line may be explained by a more efficient photoreduction process, a delayed start of the photooxidation process due to the spectral properties of incoming radiation at this low light intensity, or some other variable that we did not measure, such as wind speed. A more efficient photoprocess may not be likely, as this is further along in the experimental progress, and the DOC had already undergone some degree of photobleaching. Also

notable is the lack of a significant decrease in flux in the afternoon, which may be due to the photobleaching of DOC and its reduced capacity to produce oxidative radicals. For the entire day, the linear fit to the data is not as significant ($R^2 = 0.18$, $p = 0.05$) as that observed on July 19.

The production and buildup of DGM can be estimated from mercury flux data by calculating the DGM necessary to produce observed fluxes (see Table SI-1, Supporting Information). The fractional increase in DGM is plotted versus time (Figure SI-3, Supporting Information) to give a kinetic rate constant k for the overall net reduction reaction. For the date plotted, a k value of 0.17 h^{-1} is obtained, which is generally consistent with previously measured net photoreduction rates. For example, in a series of temperate lakes

and rivers, gross photoreduction rates ranged from 0.3 to 0.65 h⁻¹ (11). Laboratory and field experiments in freshwaters have measured photooxidation rates of 0.06 to 0.3 h⁻¹ (25, 31). Combining these two rates gives a very wide range of possible net photoreduction rates (0 to 0.59 h⁻¹), but comparing the measured general photoreduction value for lakes (0.3 h⁻¹) and photooxidation rates for a similar DOC concentration lake (0.1 h⁻¹) results in a more comparable 0.2 h⁻¹ value for net photoreduction.

Mercury Flux at Low Light. Low light intensity produced very low positive mercury flux rates. The first samples on the two diel measurement days were taken around 6:45 a.m., when irradiance was low (6 w/m² PAR, 0.15 w/m² UV-B) compared to full sun (430 w/m² PAR, 3.2 w/m² UV-B). Flux rates were the same between the +UVR and -UVR treatments at dawn on the two days, and while the -UVR treatment maintained that same value throughout the day, the +UVR treatment followed the diel pattern described above. If the low-light production rate of DGM was related to UVR, the +UVR and -UVR mesocosms should have different flux rates. The identical flux rates suggest that the production was not connected to UVR and instead might be a biologically mediated reaction. We do not have the data to differentiate between this and other possible explanations, though they have already been hypothesized and shown to exist (12).

Effects of DOC Photobleaching. During the course of the experiment, the peak mercury flux rate from the +UVR mesocosms decreased over time (Figure 4). The mesocosm with 2.5 mg/L DOC exhibited more rapid drops in mercury emission than the 1.5 mg/L DOC mesocosm. A linear regression through three points of the 2.5 mg/L DOC treatment has a slope almost 2.5 times the slope of a linear regression through the 1.5 mg/L treatment (Figure 4). The rapid decrease could be due to a number of factors, including a decrease in photoreactivity of the DOC and a decrease in the available pool of reactive mercury in the system.

Mercury flux rates declined markedly in both 1.5 and 2.5 mg/L DOC treatments. If photobleaching was responsible for the observed decreases in mercury flux rates, then there should be some observable change in optical properties in both mesocosms. However, the optical data supports photobleaching in only the 2.5 mg/L DOC treatment and not in the 1.5 mg/L treatment. The photobleaching of the 2.5 mg/L treatment may be from the degradation of chromophoric moieties in the supplementary DOC from the terrestrial wetland source that had long since been degraded in the lake water that was used for the 1.5 mg/L DOC mesocosm (32). The decrease in the most photoreactive moieties in the 2.5 mg/L DOC mesocosm apparently does not diminish the overall mercury reduction rates. The independence of mercury emission from photobleaching implies that the moieties responsible for mercury reduction are in tremendous excess in even the most photobleached DOC.

Acknowledgments

The authors wish to thank the Blooming Grove Hunting and Fishing Club at Lake Giles for their permission to conduct these experiments. We would like to acknowledge Patrick Neale at the Smithsonian Environmental Research Center for providing the SR-18 irradiance data, Craig Williamson and the IRCEB faculty for coordinating the mesocosm experiment, and Sandi Connelly for her help in the lab and in the field. The comments of three anonymous reviewers improved this manuscript. This research was funded by grants from the EPA to S.C.P. (GR-832214) and the NSF to D.P.M. (IRCEB-0210972).

Supporting Information Available

Figure illustrating the optical properties of the plastic materials used to construct the mesocosm chambers; site

location map; table of measured mercury flux rates and calculated DGM concentrations from July 19, 2005; and figure of DGM production vs. time. This material is available free of charge via the Internet at <http://pubs.acs.org>.

Literature Cited

- Xiao, Z. F.; Munthe, J.; Schroeder, W. H.; Lindqvist, O. Vertical Fluxes of Volatile Mercury over Forest Soil and Lake Surfaces in Sweden. *Tellus, Ser. B* **1991**, *43* (3), 267–279.
- Mason, R. P.; Fitzgerald, W. F.; Morel, F. M. M. The biogeochemical cycling of elemental mercury—anthropogenic influences. *Geochim. Cosmochim. Acta* **1994**, *58* (15), 3191–3198.
- Lindberg, S. E.; Stratton, W. J. Atmospheric mercury speciation: Concentrations and behavior of reactive gaseous mercury in ambient air. *Environ. Sci. Technol.* **1998**, *32* (1), 49–57.
- Gardfeldt, K.; Feng, X. B.; Sommar, J.; Lindqvist, O. Total gaseous mercury exchange between air and water at river and sea surfaces in Swedish coastal regions. *Atmos. Environ.* **2001**, *35* (17), 3027–3038.
- Lamborg, C. H.; Fitzgerald, W. F.; O'Donnell, J.; Torgersen, T. A non-steady-state compartmental model of global-scale mercury biogeochemistry with interhemispheric atmospheric gradients. *Geochim. Cosmochim. Acta* **2002**, *66* (7), 1105–1118.
- O'Driscoll, N. J.; Siciliano, S. D.; Lean, D. R. S.; Amyot, M. Gross photoreduction kinetics of mercury in temperate freshwater lakes and rivers: Application to a general model of DGM dynamics. *Environ. Sci. Technol.* **2006**, *40* (3), 837–843.
- Costa, M.; Liss, P. S. Photoreduction of mercury in sea water and its possible implications for Hg⁰ air-sea fluxes. *Mar. Chem.* **1999**, *68* (1–2), 87–95.
- Amyot, M.; Gill, G. A.; Morel, F. M. M. Production and loss of dissolved gaseous mercury in coastal seawater. *Environ. Sci. Technol.* **1997**, *31* (12), 3606–3611.
- Lalonde, J. D.; Amyot, M.; Orvoine, J.; Morel, F. M. M.; Auclair, J. C.; Ariya, P. A. Photoinduced oxidation of Hg⁰ (aq) in the waters from the St. Lawrence estuary. *Environ. Sci. Technol.* **2004**, *38* (2), 508–514.
- O'Driscoll, N. J.; Lean, D. R. S.; Loseto, L. L.; Carignan, R.; Siciliano, S. D. Effect of dissolved organic carbon on the photoproduction of dissolved gaseous mercury in lakes: Potential impacts of forestry. *Environ. Sci. Technol.* **2004**, *38* (9), 2664–2672.
- O'Driscoll, N. J.; Siciliano, S. D.; Peak, D.; Carignan, R.; Lean, D. R. S. The influence of forestry activity on the structure of dissolved organic matter in lakes: Implications for mercury photoreactions. *Sci. Total Environ.* **2006**, *366* (2–3), 880–893.
- Siciliano, S. D.; O'Driscoll, N. J.; Lean, D. R. S. Microbial reduction and oxidation of mercury in freshwater lakes. *Environ. Sci. Technol.* **2002**, *36* (14), 3064–3068.
- Garcia, E.; Amyot, M.; Ariya, P. A. Relationship between DOC photochemistry and mercury redox transformations in temperate lakes and wetlands. *Geochim. Cosmochim. Acta* **2005**, *69* (8), 1917–1924.
- Costa, M.; Liss, P. Photoreduction and evolution of mercury from seawater. *Sci. Total Environ.* **2000**, *261* (1–3), 125–135.
- Amyot, M.; Mierle, G.; Lean, D. R. S.; McQueen, D. J. Sunlight-induced formation of dissolved gaseous mercury in lake waters. *Environ. Sci. Technol.* **1994**, *28* (13), 2366–2371.
- Tseng, C. M.; Lamborg, C.; Fitzgerald, W. F.; Engstrom, D. R. Cycling of dissolved elemental mercury in Arctic-Alaskan lakes. *Geochim. Cosmochim. Acta* **2004**, *68* (6), 1173–1184.
- Xiao, Z. F.; Stromberg, D.; Lindqvist, O. Influence of humic substances on photolysis of divalent mercury in aqueous solution. *Water, Air, Soil Pollut.* **1995**, *80* (1–4), 789–798.
- Allard, B.; Arsenie, I. Abiotic reduction of mercury by humic substances in aquatic system—An important process for the mercury cycle. *Water, Air, Soil Pollut.* **1991**, *56*, 457–464.
- Krabbenhoft, D. P.; Hurley, J. P.; Olson, M. L.; Cleckner, L. B. Diel variability of mercury phase and species distributions in the Florida Everglades. *Biogeochemistry* **1998**, *40* (2–3), 311–325.
- Ferrara, R.; Mazzolai, B.; Lanzillotta, E.; Nucaro, E.; Pirrone, N. Temporal trends in gaseous mercury evasion from the Mediterranean seawaters. *Sci. Total Environ.* **2000**, *259* (1–3), 183–190.
- Poissant, L.; Amyot, M.; Pilote, M.; Lean, D. Mercury water–air exchange over the Upper St. Lawrence River and Lake Ontario. *Environ. Sci. Technol.* **2000**, *34* (15), 3069–3078.
- O'Driscoll, N. J.; Poissant, L.; Canario, J.; Ridal, J.; Lean, D. R. S. Continuous analysis of dissolved gaseous mercury and

- mercury volatilization in the Upper St. Lawrence river: Exploring temporal relationships and UV attenuation. *Environ. Sci. Technol.* **2007**, *41* (15), 5342–5348.
- (23) Kim, K. H.; Lindberg, S. E. Design and initial tests of a dynamic enclosure chamber for measurements of vapor-phase mercury fluxes over soils. *Water, Air, Soil Pollut.* **1995**, *80* (1–4), 1059–1068.
- (24) Zhang, H.; Lindberg, S. E. Air/water exchange of mercury in the Everglades I: the behavior of dissolved gaseous mercury in the Everglades Nutrient Removal Project. *Sci. Total Environ.* **2000**, *259* (1–3), 123–133.
- (25) Amyot, M.; Mierle, G.; Lean, D.; McQueen, D. J. Effect of solar radiation on the formation of dissolved gaseous mercury in temperate lakes. *Geochim. Cosmochim. Acta* **1997**, *61* (5), 975–987.
- (26) Sanemasa, I. The solubility of elemental mercury vapor in water. *Bull. Chem. Soc. Jpn.* **1975**, *48* (6), 1795–1798.
- (27) Neale, P. J. Personal communication, 2006.
- (28) Morris, D. P.; Hargreaves, B. R. The role of photochemical degradation of dissolved organic carbon in regulating the UV transparency of three lakes on the Pocono plateau. *Limnol. Oceanogr.* **1997**, *42* (2), 239–249.
- (29) McKnight, D. M.; Boyer, E. W.; Westerhoff, P. K.; Doran, P. T.; Kulbe, T.; Andersen, D. T. Spectrofluorometric characterization of dissolved organic matter for indication of precursor organic material and aromaticity. *Limnol Oceanogr.* **2001**, *46* (1), 38–48.
- (30) Sharp, J. H.; Suzuki, Y.; Munday, W. L. A comparison of dissolved organic-carbon in North-Atlantic ocean nearshore waters by high-temperature combustion and wet chemical oxidation. *Mar. Chem.* **1993**, *41* (1–3), 253–259.
- (31) Lalonde, J. D.; Amyot, M.; Kraepiel, A. M. L.; Morel, F. M. M. Photooxidation of Hg(0) in artificial and natural waters. *Environ. Sci. Technol.* **2001**, *35* (7), 1367–1372.
- (32) Osburn, C. L.; Morris, D. P.; Thorn, K. A.; Moeller, R. E. Chemical and optical changes in freshwater dissolved organic matter exposed to solar radiation. *Biogeochemistry* **2001**, *54* (3), 251–278.

Received for review April 24, 2007. Revised manuscript received July 28, 2007. Accepted August 9, 2007.

ES0709674